

# Advanced Vertical and Lateral Coupling Dynamics Control for a Four In-wheel Motor Drive Electric Vehicle

Nor El Houda Yazid<sup>1\*</sup>, Tarik Mohammed Chikouche<sup>1</sup>, Kada Hartani<sup>1</sup>, Abdelkader Merah<sup>1</sup>

<sup>1</sup> Electrotechnical Engineering Laboratory, Electrotechnical Department, Faculty of Technology, University of Saida Dr. Moulay Tahar, 20000 Ennasr, Saida, P.O.B. 138, Algeria

\* Corresponding author, e-mail: [norelhouda.yazid@univ-saida.dz](mailto:norelhouda.yazid@univ-saida.dz)

Received: 27 May 2022, Accepted: 02 November 2022, Published online: 06 December 2022

## Abstract

This paper presents an advanced vertical and lateral coupling dynamics control for stabilizing the vertical and lateral motion of a four in-wheel motor drive electric vehicle. The novelty is to investigate the possibilities of enhancing the lateral stability of electric vehicle through the correct control of their suspension system, and further improve the suspension system performances using direct yaw control (DYC) without having a contradictory effect between the vertical and lateral controllers. There are two main objectives; the first is to improve ride comfort, road holding and vehicle lateral handling performance simultaneously by using a new combined full vehicle suspension system, and the second is to strengthen electric vehicle lateral handling performance by using a sliding mode technique for controlling the direct yaw moment. For vehicle suspension system control, we are seeking to design a skyhook control to control the suspension damper and a sliding mode control to stabilize the position of the sprung masses of the in-wheel damper vibration absorber (DVA). To solve the problems caused by the chattering phenomena and ensure the exponential stability of the sprung mass, the continuous singular terminal sliding-mode controller is selected to design the sliding mode control used as a DVA controller. Simulation results show that the coordinated control between DYC and combined full vehicle suspension system under several turns' maneuvers and under random road excitations, can stabilize electric vehicle lateral motion, enhance the vehicle ride comfort, road holding, enhance the rollover resistance performance and satisfy the main suspension performances simultaneously.

## Keywords

suspension ride comfort, dynamic vibration absorber, road holding, lateral stability, vertical dynamics, lateral dynamics

## 1 Introduction

Electric vehicles (EVs) have received much interest as a potential solution to energy and environmental issues. Furthermore, the use of electric motors and inverters in EV drive trains, offer several benefits over internal combustion engines [1]. Electric vehicles may be able to achieve higher levels of safety and handling than internal combustion engines (ICEVs) due to the superior control performance of electric motors [2].

There are different vehicle dynamics control systems for vehicle movements, which may be classified into three categories: longitudinal, lateral, and vertical controls. For yaw rate control, a variety of actuators, such as active steering and active braking, could be used. The vehicle's lateral motion is controlled by the active front steering system (AFS) and the direct yaw control (DYC) system. This system provides an additive driver-independent steering angle to correct the steering angle of the vehicle's steered

wheels and affects the vehicle's handling by providing lateral forces and adjusting the tire's slip angle. Direct yaw stability control is another active control technique that is used to maintain the vehicle's stability. The DYC applies right/left braking torque depending on information from the wheel steering angle to control the vehicle's yaw movement and ensure vehicle lateral stability [3].

Unlike motors used in industrial applications, traction motors used in electric vehicles (EVs) are typically required to conduct frequent starts and stops, high rates of acceleration/deceleration, high torque and low-speed hill climbing, and low torque and high-speed cruising. Furthermore, EVs with electric motors offer three distinct advantages:

1. motor torque can be generated quickly and precisely;
2. electric motors can be mounted in each wheel;
3. motor torque can be precisely measured [4–6].

Unfortunately, the incorporation of electric motors into the wheels of electric vehicles increases the unsprung mass, which has an effect on the vehicle's road holding and ride comfort. This effect appeared when comparing the system's performance with a conventional tire and a tire with an in-wheel electric motor [7]. Suspensions in electric vehicles with In-Wheel Motors (IWMs) become IWM-suspension systems which have been the subject of considerable research over the past decades [8–11]. The effects of IWM on suspension vertical response were investigated in [12], and a modified current chopping controller was designed to enhance system vertical performance.

The passenger comfort and vehicle control are the two main purposes of any automobile suspension. The vehicle's passengers are kept comfortable by isolating them from the irregularities in the pavement surface. Control is achieved by preventing excessive rolling and pitching of the vehicle body, as well as maintaining good contact between the tire and the road [13].

Generally, there are two solutions for reducing the vibration caused by the increased unsprung mass: an active suspension system and a dynamic vibration absorber. Many control approaches have been done in the field of robust control for active suspension systems, which is becoming a more essential priority in vehicle safety. An active suspension was proposed in [14] to decrease body roll and consequently rollover propensity. In [15, 16], a fuzzy logic controller (FLC) applied to active suspension system is optimized with particle swarm optimization (PSO). By combining fuzzy logic with sliding mode control (SMC), the chattering phenomena that occur in SMC is eliminated. [17] used an adaptive neuro-fuzzy based sliding mode control for full car active suspension system. In [18], an active suspension system is presented that combines sliding mode control with a disturbance observer. In [19], a backstepping control is proposed for active suspension system. In [20], a nonlinear controller is used for dual objective suspension system. Some applications of Lyapunov functions based controllers can be found in [21, 22]. Sliding-mode controllers are insensible to several types of disturbances and are well-known for their excellent robust performance [23]. The main disadvantage is that the discontinuous structure of the control signals causes very high frequency oscillations, which is known as chattering. [24] investigated at how to mitigate this phenomenon using approximations for discontinuous signals. Continuous sliding-modes controllers are another way to mitigate chattering's effects [25, 26]. [27] presents an adaptive damping system (ADS) that

improve the vibration effect of the vertical motion for the vehicle considering the longitudinal motion of the vehicle body. In [28], a novel skyhook preview control (SPC) approach is adopted to identify the transient road to preview a semi-active suspension that can effectively enhance the ride comfort of the vehicle.

As for the DVA, [29] used an actuator between the sprung and unsprung mass to synthesize active control force for the controlled suspension system. For the IWM application of switched reluctance motor (SRM), [11] developed a new approach for vibration mitigation based on a dynamic vibration absorbing structure (DVAS). Many innovative approaches are used in the literature to improve the ride quality, handling, and control performance of electric vehicles [30]. [31] presented an integration design scheme and an optimization control strategy for electric wheels, in which we find linear quadratic regulator (LQR) method for a suspension actuator force control and alterable-domain-based fuzzy control method for the DVA actuator force control.

The purpose of this paper is to achieve a better ride comfort, road holding and a good lateral stability for a four in-wheel motor drive electric vehicle using advanced vertical and lateral coupling dynamics control. In reality, improving both ride comfort and road holding objectives in a controlled manner simultaneously is impossible [32, 33]. To overcome this problem, a proposed combined suspension control based on the aspect of compromise between ride comfort and road holding has been developed in this study. Therefore, we are seeking to control the suspension damper with a skyhook controller and a continuous singular terminal sliding-mode controller for the in-wheel DVA.

This paper is arranged as follows: after citing the recent surveys on the direct yaw control (DYC), the dynamic vibration absorber (DVA) and active suspension systems in the introduction, the dynamic model of full vehicle active suspension taking into account the vehicle's lateral motion is presented in Section 2. The design of the advanced vertical and lateral coupling dynamics control is developed in Section 3. At the beginning we present the optimization of the DVA system's parameters using sequential quadratic programming (SQP) algorithm. Then, the design of the combined full vehicle suspension system control based on in-wheel dynamic vibration absorber and active vehicle suspension is presented. This combined control combines skyhook suspension control and continuous singular terminal sliding mode control, for improvements in vehicle ride comfort performance and the road holding ability. At the end, we develop the direct yaw control that uses sliding

mode control to improve road handling by adding an additional yaw moment. Section 4 presents some simulation results, while Section 5 concludes with some remarks.

## 2 In-wheel motor drive EV dynamic model

There are various possible IWM-driven EV structures regarding the electric propulsion and the energy sources. Fig. 1 shows the structure studied in this work, where all in-wheel PMS motors are fed through a five-leg inverter.

An established 16-degree-of-freedom coupling dynamic model is given to investigate the coupling dynamics control in the vertical and lateral directions of in-wheel motor (IWM)-driven electric vehicle under steering input and random road excitation. The physical full vehicle active suspension model with the DVA-based electric wheel is shown in Fig. 2, where the in-wheel motor is suspended from both the sprung mass and unsprung mass by a passive mechanism of "spring-damper" systems, and two controlled active forces are applied to the in-wheel with DVA and suspension.

Based on the Newton's second law, the motion equations of the four unsprung masses (wheels), sprung mass (vehicle body), and DVA-based electric wheel can be written as [31, 34]:

The vertical motion of the vehicle body is:

$$m_s \ddot{z}_s = F_{t1} + F_{t2} + F_{t3} + F_{t4}, \quad (1)$$

where:

$$\begin{cases} F_{t1} = -k_{s1}(z_{s1} - z_{w1}) - c_{s1}(\dot{z}_{s1} - \dot{z}_{w1}) + k_{d1}(z_{m1} - z_{w1}) + F_{a1} \\ F_{t2} = -k_{s2}(z_{s2} - z_{w2}) - c_{s2}(\dot{z}_{s2} - \dot{z}_{w2}) + k_{d2}(z_{m2} - z_{w2}) + F_{a2} \\ F_{t3} = -k_{s3}(z_{s3} - z_{w3}) - c_{s3}(\dot{z}_{s3} - \dot{z}_{w3}) + k_{d3}(z_{m3} - z_{w3}) + F_{a3} \\ F_{t4} = -k_{s4}(z_{s4} - z_{w4}) - c_{s4}(\dot{z}_{s4} - \dot{z}_{w4}) + k_{d4}(z_{m4} - z_{w4}) + F_{a4} \end{cases} \quad (2)$$

The pitch motion of the vehicle body is:

$$J_y \ddot{\theta} = l_r (F_{t3} + F_{t4}) - l_f (F_{t1} + F_{t2}). \quad (3)$$

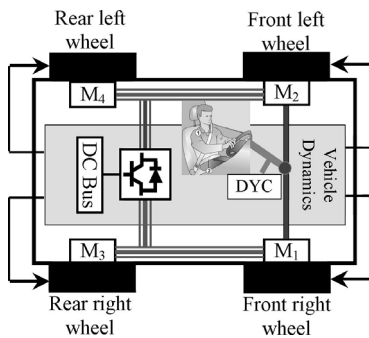


Fig. 1 Configuration of the four in-wheel motor drive EV

The roll motion of the vehicle body is:

$$J_x \ddot{\phi} = m_s v_x (\dot{\beta} + r) h + m_s g h \theta + (F_{t1} + F_{t2} + F_{t3} + F_{t4}) \frac{d}{2}. \quad (4)$$

The yaw motion of the vehicle is:

$$J_z \dot{r} = l_f (F_{yf1} + F_{yf2}) - l_r (F_{yr3} + F_{yr4}). \quad (5)$$

The lateral motion of the vehicle is:

$$m_{tot} v_x (\dot{\beta} + r) = F_{yf1} + F_{yf2} + F_{yr3} + F_{yr4} + m_s h \ddot{\phi}. \quad (6)$$

The vertical motion of each wheel (the unsprung masses) is:

$$\begin{cases} m_w \ddot{z}_{w1} = -F_{t1} - k_{w1}(z_{w1} - z_{r1}) - c_{d1}(\dot{z}_{m1} - \dot{z}_{w1}) \\ m_w \ddot{z}_{w2} = -F_{t2} - k_{w2}(z_{w2} - z_{r2}) - c_{d2}(\dot{z}_{m2} - \dot{z}_{w2}) \\ m_w \ddot{z}_{w3} = -F_{t3} - k_{w3}(z_{w3} - z_{r3}) - c_{d3}(\dot{z}_{m3} - \dot{z}_{w3}) \\ m_w \ddot{z}_{w4} = -F_{t4} - k_{w4}(z_{w4} - z_{r4}) - c_{d4}(\dot{z}_{m4} - \dot{z}_{w4}) \end{cases} \quad (7)$$

The vertical motion of each motor is:

$$\begin{cases} m_m \ddot{z}_{m1} = -k_{d1}(z_{m1} - z_{w1}) - c_{d1}(\dot{z}_{m1} - \dot{z}_{w1}) + F_{DAV1} \\ m_m \ddot{z}_{m2} = -k_{d2}(z_{m2} - z_{w2}) - c_{d2}(\dot{z}_{m2} - \dot{z}_{w2}) + F_{DAV2} \\ m_m \ddot{z}_{m3} = -k_{d3}(z_{m3} - z_{w3}) - c_{d3}(\dot{z}_{m3} - \dot{z}_{w3}) + F_{DAV3} \\ m_m \ddot{z}_{m4} = -k_{d4}(z_{m4} - z_{w4}) - c_{d4}(\dot{z}_{m4} - \dot{z}_{w4}) + F_{DAV4} \end{cases} \quad (8)$$

The vertical motion of each corner is expressed as:

$$\begin{cases} z_{s1} = z_s - l_f \phi - \frac{d}{2} \theta \\ z_{s2} = z_s - l_f \phi + \frac{d}{2} \theta \\ z_{s3} = z_s + l_r \phi - \frac{d}{2} \theta \\ z_{s4} = z_s + l_r \phi + \frac{d}{2} \theta \end{cases} \quad (9)$$

where:

- $z_s$ : vertical displacement of the sprung mass;
- $\theta$ : pitch motions;
- $\phi$ : roll motions;
- $r$ : yaw rate velocity of vehicle;
- $\beta$ : the sideslip angle of the vehicle;
- $z_{si}$ : the vertical displacement of the junction between the  $i^{\text{th}}$  sub-suspension and vehicle body;
- $z_{wi}$ : vertical displacement of the wheel;
- $z_{mi}$ : vertical displacement of the electric motor;
- $r_i$ : the road excitation to the corresponding tire;
- $\ddot{z}_s$ : vertical acceleration of the sprung mass;
- $\ddot{\theta}$ : pitch acceleration;
- $\ddot{\phi}$ : roll acceleration;
- $\ddot{z}_{wi}$ : vertical acceleration of the wheel;

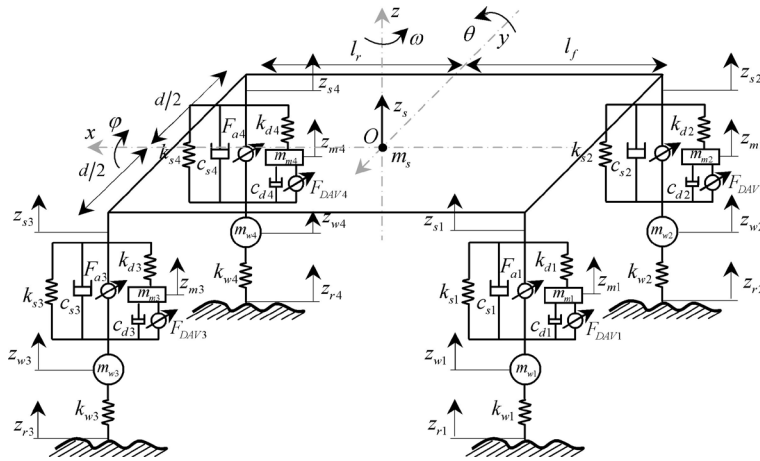


Fig. 2 Structure of full vehicle active suspension with IWM

- $F_{ti}$ : equivalent force of  $i^{\text{th}}$  in-wheel motor;
- $F_{si}$ : the spring force;
- $F_{di}$ : the damping force;
- $F_{wi}$ : the spring force (tire);
- $F_{sDAVi}$ : the spring force (DAV);
- $F_{ai}$ : the active force exerted by a suspension actuator;
- $F_{DAVi}$ : the active force exerted by an actuator (DAV);
- $i = 1, 2, 3, 4$ : front right (FR), front left (FL), rear right (RR), rear left (RL), and the parameter values of full vehicle active suspension with IWM are defined in Table 1.

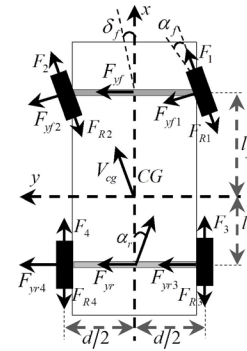


Fig. 3 Lateral dynamic model

The sideslip angles for the front and rear axles for vehicle can be expressed as follows:

$$\alpha_f = \beta + \frac{l_f}{v_x} r - E_f \theta - \delta_f, \quad (10)$$

$$\alpha_r = \beta - \frac{l_r}{v_x} r - E_r \theta,$$

where  $v_x$ : longitudinal velocity of vehicle in body reference frame;  $\delta_f$ : steering angle of front tires.

With a linear tire model, the front and rear cornering forces can be expressed as the product of the cornering stiffness ( $K_{yf}$ ,  $K_{yr}$ ) and the sideslip angle ( $\alpha_f$ ,  $\alpha_r$ ), Fig. 3.

$$\begin{aligned} F_{yf1} = F_{yf2} &= -K_{yf} \alpha_f \\ F_{yr3} = F_{yr4} &= -K_{yr} \alpha_r \end{aligned} \quad (11)$$

### 3 Design of advanced vertical and lateral coupling dynamic control

Fig. 4 shows the integrated full vehicle suspension system control which mainly includes the following two aspects, while satisfying the four main suspension performances listed below [11]. The DVA actuator force is controlled by using sliding mode control method to further reduce

the motor vertical vibration, the suspension actuator force is controlled by using skyhook control to improve vehicle ride comfort, and direct yaw control that uses sliding mode control to improve road handling:

- *Ride comfort*: it can be evaluated by the sprung mass acceleration  $SMA = \ddot{z}_s$ .
- *Rattle space* (suspension deflection): when designing a suspension, it is important to minimize the rattle space which can be evaluated by  $RS_i = z_{si} - z_{wi}$ .
- *Road holding*: the tire deflection (TD) is used as a representative measurement of the road holding which is defined as:  $TD_i = z_{wi} - z_{ri}$ . In order to obtain better steering ability, acceleration and braking when driving in worse road conditions, the TD should be small.
- *Stator acceleration*: in order to minimize the vibrations of the wheel and consequently improve the ride comfort, it is necessary to minimize the stator acceleration (SA)  $SA_i = \ddot{z}_{mi}$ .

#### 3.1 Parameters optimization of the in-wheel DVA using SQP algorithm

Note that the sequential quadratic programming (SQP) algorithm is well suited for constrained design optimizations [35]. In our work, we will use this algorithm to

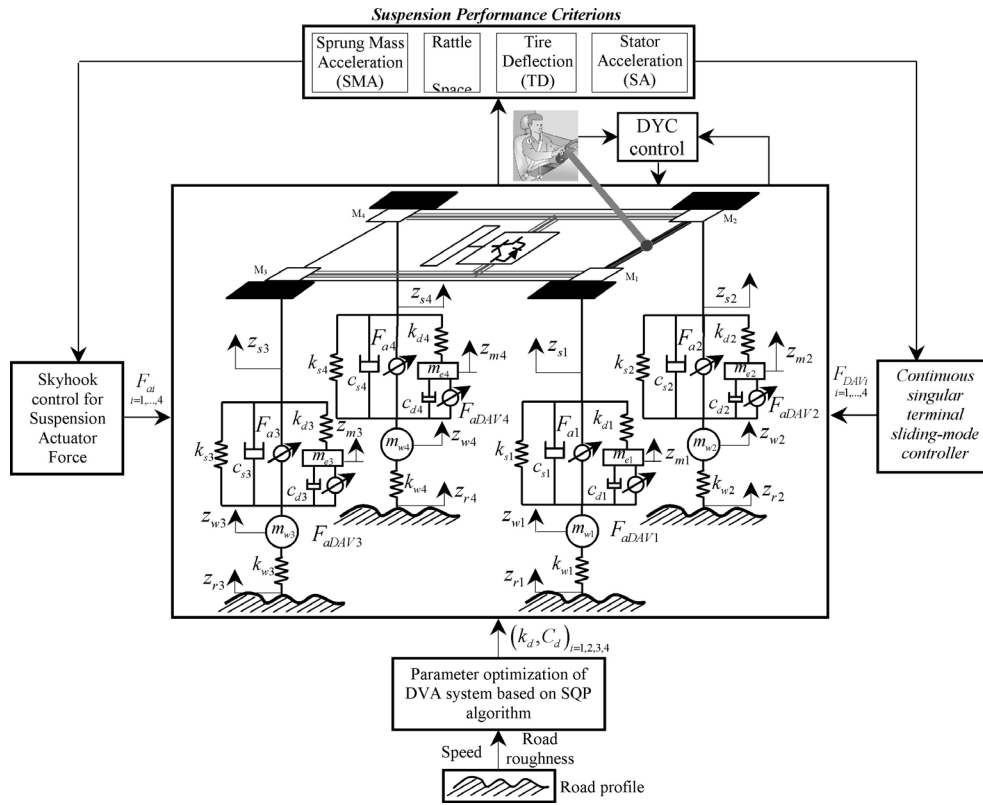


Fig. 4 Integrated full vehicle suspension system control

reduce the vibrations of the stator and the deflection of the suspension, the parameter optimization problem with the SQP method can be written as a penalty function:

$$\left\{ \begin{array}{l} \min J(k_d, c_d) = \alpha_1 \frac{\text{RMS}(\text{SMA}_{\text{DAV}})}{\text{RMS}(\text{SMA}_{\text{con}})} + \dots \\ + \alpha_2 \frac{\text{RMS}(\text{RS}_{\text{DAV}})}{\text{RMS}(\text{RS}_{\text{con}})} + \alpha_3 \frac{\text{RMS}(\text{TD}_{\text{DAV}})}{\text{RMS}(\text{TD}_{\text{con}})} + \dots \\ + \alpha_4 \frac{\text{RMS}(\text{SA}_{\text{DAV}})}{\text{RMS}(\text{SA}_{\text{con}})} \\ \text{RMS}(q) = \sqrt{\frac{1}{n} \sum_i q_i^2} \end{array} \right. , \quad (12)$$

where  $\text{SMA}_{\text{DAV}}$ ,  $\text{RS}_{\text{DAV}}$ ,  $\text{TD}_{\text{DAV}}$ , and  $\text{SA}_{\text{DAV}}$  are the expression of the four evaluation indexes in the electric wheel with the DVA,  $\text{SMA}_{\text{con}}$ ,  $\text{RS}_{\text{con}}$ ,  $\text{TD}_{\text{con}}$ , and  $\text{SA}_{\text{con}}$  are those in the conventional electric wheel.  $\text{RMS}(q)$  means the root mean square values of signal  $q$ , which can reduce the random influences in a certain extent and  $n$  is number of measurements.  $\alpha_1$ ,  $\alpha_2$ ,  $\alpha_3$  and  $\alpha_4$  are the penalty factors for each of the four indexes, and  $\alpha_1 + \alpha_2 + \alpha_3 + \alpha_4 = 1$ .

The sprung mass acceleration (SMA) and stator acceleration (SA) are considered important than the rattle space (RS) and tire deflection (TD). Thus, the four penalty factors are set to:  $\alpha_1 = 0.3$ ,  $\alpha_2 = 0.15$ ,  $\alpha_3 = 0.15$  and  $\alpha_4 = 0.4$ . The op-

timal values of and can be found by substituting the aforementioned penalty factors in Eq. (12). These values are shown in Table 1.

### 3.2 Vertical control based on combined in-wheel DVA and suspension actuators control

#### 3.2.1 Design of SMC for in-wheel DVA

In our study, a structure of sliding mode controller, called continuous singular terminal sliding-mode control (CSTA), is proposed for DVA force control to suppress the motor vibration and obtain optimal performances, Fig. 5.

The vertical motion of each motor is:

$$\left\{ \begin{array}{l} m_{mi} \ddot{z}_{mi} = -k_{di} (z_{mi} - z_{wi}) - c_{di} (\dot{z}_{mi} - \dot{z}_{wi}) + u_i + \gamma(t) \\ F_{\text{DAVi}} = u_i \\ \left\| \frac{d}{dt}(\gamma(t)) \right\|_{\infty} \leq \eta, \eta > 0 \end{array} \right. . \quad (13)$$

The control law is composed of two controllers: a nominal controller and robust controller.

$$u_i = u_{ni} + u_{ri} \quad (14)$$

Thus, consider the following nominal controller:

$$u_{ni} = k_{di} (z_{mi} - z_{wi}) + c_{di} (\dot{z}_{mi} - \dot{z}_{wi}). \quad (15)$$

**Table 1** EV dynamic model parameters

Definition	Symbol	Value	Unit
Mass of the vehicle	$m_{tot}$	1030	kg
Mass of the vehicle body	$m_s$	928.2	kg
Mass of front left and right wheel	$m_{w1}, m_{w2}$	26.5	kg
Mass of rear left and right wheel	$m_{w3}, m_{w4}$	24.4	kg
Mass of front left and right stator	$m_{m1}, m_{m2}$	26.5	kg
Mass of rear left and right stator	$m_{m3}, m_{m4}$	24.4	kg
Roll moment of the inertia of the vehicle body	$J_x$	300	kg·m <sup>2</sup>
Pitch moment of the inertia of the vehicle body	$J_y$	1058	kg·m <sup>2</sup>
Yaw moment of the inertia of the vehicle body	$J_z$	1087	kg·m <sup>2</sup>
Damping of front left and right DVA	$c_{d1}, c_{d2}$	480	N/(m/s)
Damping of rear left and right DVA	$c_{d3}, c_{d4}$	480 × 0.84	N/(m/s)
Stiffness of front left and right DVA	$k_{d1}, k_{d2}$	8025	N/m
Stiffness of rear left and right DVA	$k_{d3}, k_{d4}$	8025 × 0.84	N/m
Stiffness of front left and right wheel	$k_{w1}, k_{w2}$	192000	N/m
Stiffness of rear left and right wheel	$k_{w3}, k_{w4}$	192000	N/m
Damping of front left and right suspension	$c_{s1}, c_{s2}$	1800	N/(m/s)
Damping of rear left and right suspension	$c_{s3}, c_{s4}$	1500	N/(m/s)
Stiffness of front left and right/rear left and right	$k_{s1}, k_{s2}$	25000	N/m
Stiffness of front left and right/rear left and right	$k_{s3}, k_{s4}$	22000	N/m
Distance between mass center and front axle	$l_f$	0.908	m
Distance between mass center and rear axle	$l_r$	1.392	m
Distance between mass center and the axis of the roll	$h$	1.392	m
Wheel track	$d$	1.392	m
Roll steering coefficient of front tire	$E_f$	-0.114	-
Roll steering coefficient of rear tire	$E_r$	0	-
Ratle space	$L$	0.12	m
Lateral stiffness of front tire cornering	$K_{yf}$	35000	N/m
Lateral stiffness of rear tire cornering stiffness	$K_{yr}$	35000	N/m

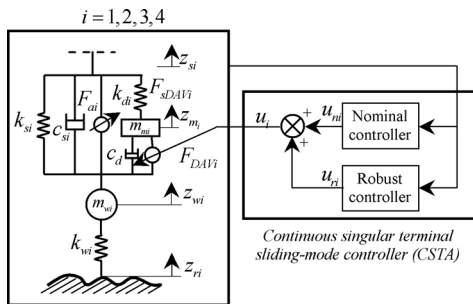


**Fig. 5** Structure of proposed active control system using CSTA

The problem now is to design  $u_{ri}$  to ensure that  $z_{mi}$  tends to zero in the presence of the disturbance term  $\gamma(t)$ , using a continuous control law while ensuring the stability of the dynamics for  $\dot{z}_{mi}$ ,  $z_{wi}$  and  $\dot{z}_{wi}$ .

Define the following function:

$$s_i = m_{mi} z_{mi}. \tag{16}$$

Thus, from Eqs. (13) to (16), it follows that:

$$\ddot{s}_i = u_{ri} + \gamma(t). \tag{17}$$

It is clear that the relative degree of  $s_i$  with respect to  $\gamma(t)$  is equal to two. Moreover, the task has been reduced to robustly stabilize the system (Eq. (17)).

In order to design the robust controller  $u_{ri}$  with the continuous singular terminal sliding-mode control (CSTA), the following assumption is introduced [36, 37]:

$$\begin{aligned} \sigma &= k_\sigma [s]^{2/3} + \dot{s}, \\ u_r &= -k_1 [\sigma]^{1/2} + \ddot{v}, \\ \ddot{v} &= -k_2 [\sigma]^0, \end{aligned} \tag{18}$$

where:  $k_\sigma > 0$ ,  $k_1 = 1.5 \eta^{1/2}$ ,  $k_2 = 1.1 \eta$ .

Notice that the used control law that drives our vehicle suspension system is continuous in nature, and no chattering will influence the system theoretically [38].

### 3.2.2 Design of skyhook control for active suspension system

In fact, the DVA system, when installed in parallel with the vehicle suspension, changes the vehicle's vibration characteristics, deteriorates the vibrations of the suspended mass and weakens the original suspension's performance. Therefore, an appropriate suspension control is required. In Section 3.2.2, we use a single controller structure based on the skyhook with an exponentially variable damper to control the suspension actuator force while simultaneously improving vehicle ride comfort and road holding.

Skyhook suspension is a concept in which a sprung mass can be maintained in a stable position by an imaginary straight line or an imaginary force. Obviously, a vehicle is attached to the ground through a spring and damper in a passive suspension system. Skyhook suspension achieves better stability than passive suspension. The actuator will be regulated where it will meet with skyhook theory in the scenario when the damper coefficient is entirely matching the imaginary line or the imagined force. In basic skyhook model where damper has fixed value, we get good ride comfort because velocity component of unsprung mass is not included into the system dynamics. However, we have to compromise on road holding and relative suspension deflection (RSD) of sprung and unsprung masses. To achieve good ride comfort, good RSD a skyhook model with variable damper is used [39].

In this model, the skyhook damper which is varied exponentially according to relative suspension deflection (RSD) and decreasing at the same time that RSD is growing. It is given as:

$$b_{sky} = b \times e^{-k_1 \varepsilon} \quad (19)$$

Notice that  $k_1$  is chosen constant to vary the damper coefficient.

All unknown coefficients in Eq. (19) are estimated by particle swarm optimization (PSO) method.

Relative suspension deflection is defined by the relative motion ratio of sprung mass and unsprung mass  $z_{si} - z_{wi}$  to the rattle space  $L$ . It should always be less than unity which is denoted by:

$$\varepsilon = \frac{z_{si} - z_{wi}}{L} \quad (20)$$

The control signal is given as below:

$$F_{ai} = -b_{sky} \times \dot{z}_{si} \quad (21)$$

### 3.3 Lateral control based on DYC using sliding mode control

To enhance more the lateral stability, lateral control and handling performance of the electric vehicle, the DYC system provides a corrective yaw moment to move the vehicle's states to the reference region while controlling the sideslip angle. It uses the yaw rate error and vehicle sideslip angle error as input variables and corrective yaw moment as output variable. The structure of the proposed DYC is shown in Fig. 6. We are going to use a sliding mode controller to follow a desired course, seeking to keep the error between the actual vehicle yaw rate ( $r$ ) and the desired yaw rate ( $r_d$ ) to zero; i.e., the controller must follow the driver's intended reference yaw rate by reducing the tracking error between the actual and desired yaw rates to zero. The reference model for yaw rate  $r_d$  is a function of the steering angle of the front wheel angle  $\delta_f$  given by Eq. (22) [4]:

$$r_d = \frac{k_r}{1 + \tau s} \delta_f(s), \quad (22)$$

where:

$$k_r = \frac{v_x}{l_f + m_{tot} l_f l_r v_x^2 / 2l_f (l_f + l_r) K_{yr}}, \quad (23)$$

$$\tau = \frac{J_v v_x}{m_{tot} l_r v_x^2 + 2K_{yr} l_f (l_f + l_r)}. \quad (24)$$

Here,  $k_r$  is the stability factor,  $\tau$  is the desired time constant.

The yaw rate error between the actual vehicle yaw rate ( $r$ ) and the desired yaw rate ( $r_d$ ) is defined by Eq. (25):

$$e_r = r - r_d. \quad (25)$$

We choose the sliding surface as follows:

$$S = e_r + \lambda \dot{e}_r. \quad (26)$$

The dynamics of sliding motion is governed by:

$$\begin{aligned} S = 0 &\Rightarrow e_r + \lambda \dot{e}_r = 0 \\ &\Rightarrow (r - r_d) + \lambda (\dot{r} - \dot{r}_d) = 0 \\ &\Rightarrow (r - r_d) + \lambda (a_{21} v_y + a_{22} r + b_2 \delta_f - \dot{r}_d) = 0, \end{aligned} \quad (27)$$

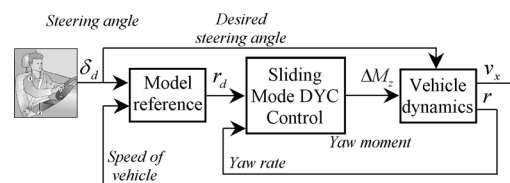


Fig. 6 Block diagram of DYC with sliding mode control

where:

$$a_{11} = -2 \frac{K_{yf} + K_{yr}}{M_v v_x}, \quad a_{12} = 2 \frac{-K_{yf} l_f + K_{yr} l_r}{M_v v_x} - v_x,$$

$$a_{21} = 2 \frac{-K_{yf} l_f + K_{yr} l_r}{J_v v_x}, \quad a_{22} = -2 \frac{K_{yf} l_f^2 + K_{yr} l_r^2}{J_v v_x},$$

$$b_2 = \frac{2K_{yf} l_f}{J_v}.$$

So, the expression of the equivalent control:

$$M_{zeq} = -\frac{1}{cb_2} \left[ (r - r_d) + c(a_{21}v_y + a_{22}r - b_2\delta_f \dot{r}_d) \right]. \quad (28)$$

If the states of the system have not reached the sliding surface, the equivalent control must be reinforced by another so-called robust control, then we define the resulting corrective yaw moment by:

$$\Delta M_z = M_{zeq} - M_{zrob} \cdot \text{sgn}(S). \quad (29)$$

Let's replace the "Sign" function with the "Saturation" function to mitigate the "Chattering" effects. The resulting steering angle becomes:

$$M_z = M_{zeq} - M_{zrob} \cdot \text{sat}(S). \quad (30)$$

We therefore define the corrective yaw moment such that:

$$\Delta M_z = -\frac{1}{cb_2} \left[ (r - r_d) + c(a_{21}v_y + a_{22}r + b_2\delta_f - \dot{r}_d) \right] - \dots$$

$$\dots - \frac{\eta}{b_2} \text{sat}(S). \quad (31)$$

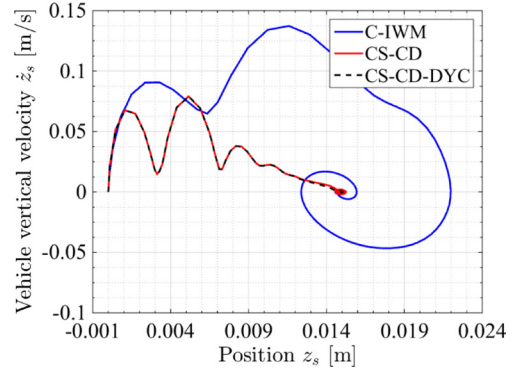
### 3.4 Stability analysis

Phase plane analysis is graphical analysis and the solution trajectories can be represented by curves in a plane. This method is used in our work because it provides easy visualization of the system qualitative without solving the nonlinear equations analytically where we can study the behavior of the nonlinear system from various initial conditions. The equilibrium point  $x^* = x_0$  of a system starting at an initial condition  $x(t_0) = x_0$  is said to be stable (in the sense of Lyapunov stability) or motion of the system about its equilibrium point is said to be stable if the system states ( $x$ ) is perturbed away from  $x_0$  then it stays close to  $x_0$ . Mathematically  $x_0$  is stable if, for any radius  $R > 0$ . There exists some radius  $r(R) > 0$  as follows:

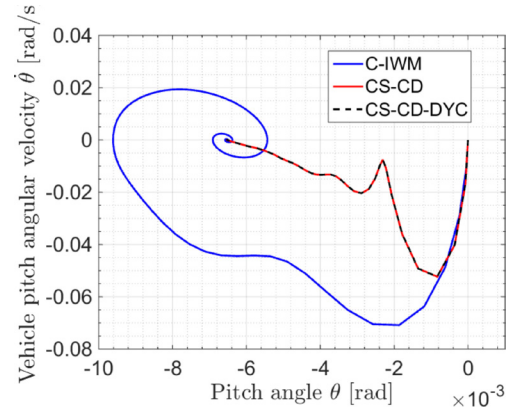
$$\|x_0\| < r \Rightarrow \|x\| < R, \forall t \geq t_0. \quad (32)$$

Otherwise, the equilibrium point is unstable.

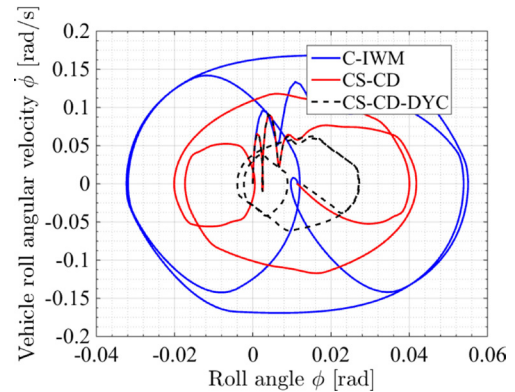
The notion of stability basically states that given a system with a close beginning condition, the system's trajectory can be kept arbitrarily close to it [40]. The different trajectories presented in the phase planes for both the passive and active suspension systems with the DYC controller, were obtained by applying step inputs to the tires in different configurations, Fig. 7. In Fig. 7(a), the step inputs



(a)



(b)



(c)

**Fig. 7** Phase planes: (a) vehicle vertical velocity vs. position; (b) vehicle pitch angular velocity vs. pitch angle; (c) vehicle roll angular velocity vs. roll angle. C-IWM: Conventional electric wheel; CS-CD: controlled suspension + controlled DVA-based electric wheel. CS-CD-DYC: controlled suspension + controlled DVA-based electric wheel + direct yaw control

have been applied to all tires at the same time, and for Figs. 7(b) and (c), the step inputs have been applied to only front tires and only left tires, respectively.

The trajectories converge to the equilibrium point, as shown in Fig. 7, demonstrating that the proposed controller's outperforms the passive system in terms of energy dissipation. The phase planes demonstrate that the active suspension system is Lyapunov asymptotically stable. Other method of the convergence proofs of the given continuous sliding-modes controllers can be found in [36].

#### 4 Simulation results and discussion

In Section 4, the proposed full vehicle suspension system, which is based on the combination of continuous singular terminal sliding-mode controller for DVA system, Skyhook controller for active suspension system and sliding mode controller for DYC system, is implemented on MATLAB & Simulink software under several turns' maneuvers and under random road excitations at the same time, to validate the lateral stability enhancing, the ride comfort performance and the road holding ability of a four in-wheel motor drive electric vehicle. The parameters of this model are listed in Table 1 [41].

Performance of the proposed controllers system has been evaluated under three tests by comparing results of the following terms of the electric wheel configuration, DVA control method, suspension control method and DYC control method as shown in Table 2.

The irregularities in the pavement surface are characterized as road profile, often known as road roughness or road unevenness, which is one of the most important inputs of vehicle systems, and it may have a significant impact on vehicle performance in terms of ride comfort and road handling [42, 43]. In this work, a random road excitation of class C is used to validate the better ride performance of active suspension system with DVA and DYC controllers.

**Table 2** Full-vehicle model with different three tests

N°	Test	DVA control	Suspension control	DYC
1	Conventional electric wheel (C-IWM)	–	No control	No control
2	Controlled Suspension + Controlled DVA-based electric wheel (CS –CD)	CSTA control	Skyhook control	No control
3	Controlled Suspension + Controlled DVA-based electric wheel + Direct Yaw Control (CS-CD-DYC)	CSTA control	Skyhook control	Sliding mode control

According to ISO 8601 [44], the power spectral density (PSD) of the random road excitation can be defined as:

$$G_q(n) = G_q(n_0) \left( \frac{n}{n_0} \right)^{-w}, \quad (33)$$

where  $n$  is the spatial frequency,  $n_0$  is the reference spatial frequency with the value of  $n_0 = 1 \text{ rad}\cdot\text{m}^{-1}$  and  $G_q(n_0)$  is the PSD for the reference spatial frequency, determined by road class.  $w$  is frequency index, usually ( $w = 2$ ), ( $v_x$ ) is the vehicle speed, and  $w(t)$  stands for the white noise disturbance of the road.

The definition of road class given by ISO 8608:2016 [45] is shown in Table 3.

The random road excitation is determined by filtering a white noise model and the vehicle speed is kept as (80 km/h):

$$\dot{z}_{r,1,2}(t) = -2\pi V_x n_0 z_{r,1,2}(t) + \sqrt{G_q(n_0) V_x} W(t). \quad (34)$$

The road condition for the rear wheel is the same as the front wheel but with a time delay of.

The random road excitation for the front and the rear wheels and the steering wheel angle input are taken as excitation sources acting on the vehicle coupling dynamic model, Figs. 8 and 9. The simulation results including lateral and vertical vehicle dynamics behaviors are shown in Figs. 10 to 20.

In reality, the vehicle can follow a variety of trajectories depending on the geometry of the road. In our simulation case, the vehicle will follow a succession of turns [4] with a constant speed, i.e. 80 km/h, and then follow a straight road with the same speed (see Fig. 9), in the presence of vibrations

**Table 3** Road class definition

Class	$G_q(n_0) 10^{-6} \text{ m}^3$
A	16
B	64
C	256

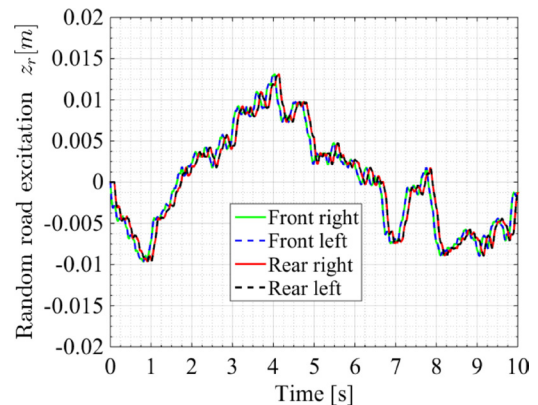


**Fig. 8** Random road excitation

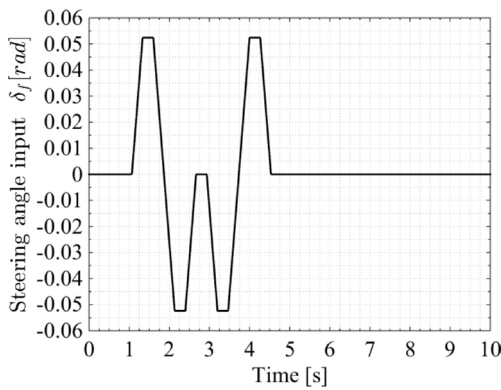


Fig. 9 Steering angle input

resulting from irregularities in the road [42, 43], i.e. vertical movements of the road exerted on the tires, Fig. 8. Table 4 summarizes the various situations that arise while driving.

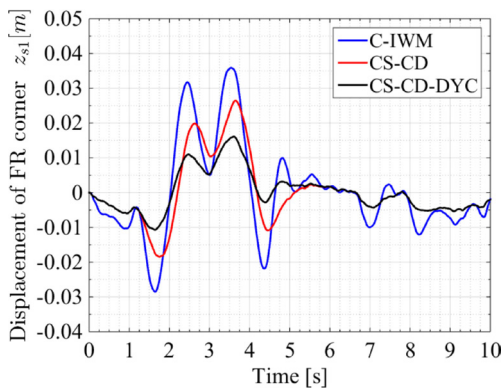
Modal assessment is used to evaluate the natural frequencies of the electric vehicle equipped with four C-IWMs model [46]. A MATLAB code has also been created to compute the Eigen-values of the suspension systems. Eigen-values give information about natural frequencies. Table 5 summarizes the results obtained using a modal assessment and the results estimated by simulation.

Table 6 shows the Root Mean Square (RMS) comparison of the vehicle dynamic responses under random road

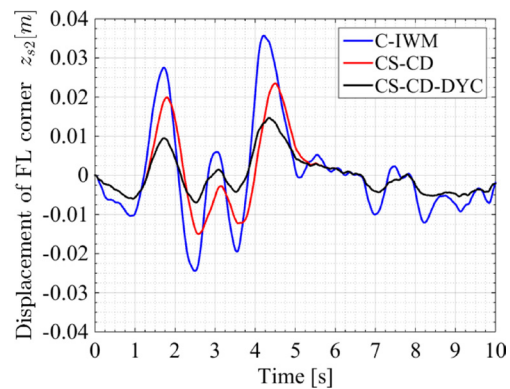
excitation. The percentages of improvement change compared to passive suspension system are also listed in parenthesis. Smaller values for RMS mean an improvement in related parameter, while larger values state deterioration.

According to Figs. 10 and 11 and Table 6, the vertical acceleration and displacement of each corner (front left/right and rear left/right) are considerably reduced in the CS-CD case compared to the C-IWM case. This indicates that the Skyhook control designed for all four vehicle suspensions provides better response for the vertical dynamics of each corner of the vehicle. We notice a significant improvement in the case of CS-CD-DYC when applying the maneuvers on the steering wheel (i.e. during the period of 1–4.5 sec). When the vehicle is traveling in a straight road during a period of 4.5–10 sec, a similar response for both cases CS-CD and CS-CD-DYC is obtained. This shows that the good control of the vehicle yaw moment considerably improves the suspension performance (accelerations and vertical displacements). Note that CS-CD-DYC has slightly better performance compared to C-IWM and CS-CD, especially in the natural frequency band.

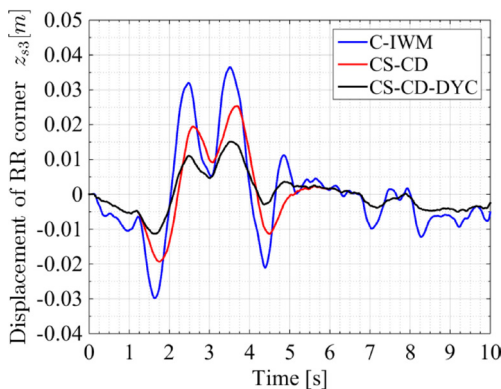
According to Figs. 12 and 13 and Table 6, the vertical acceleration and displacement of each motor (front left/right and rear left/right) are considerably reduced in the CS-CD case



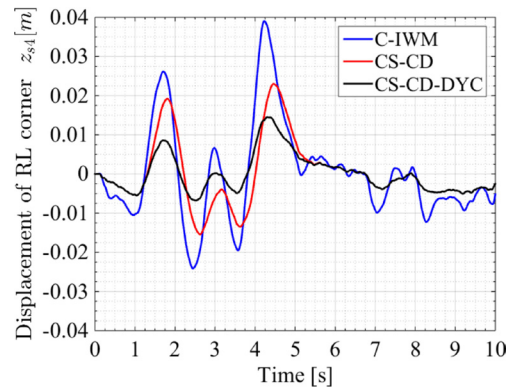
(a)



(b)



(c)



(d)

Fig. 10 Displacement of each corner: (a) front right; (b) front left; (c) rear right; (d) rear left

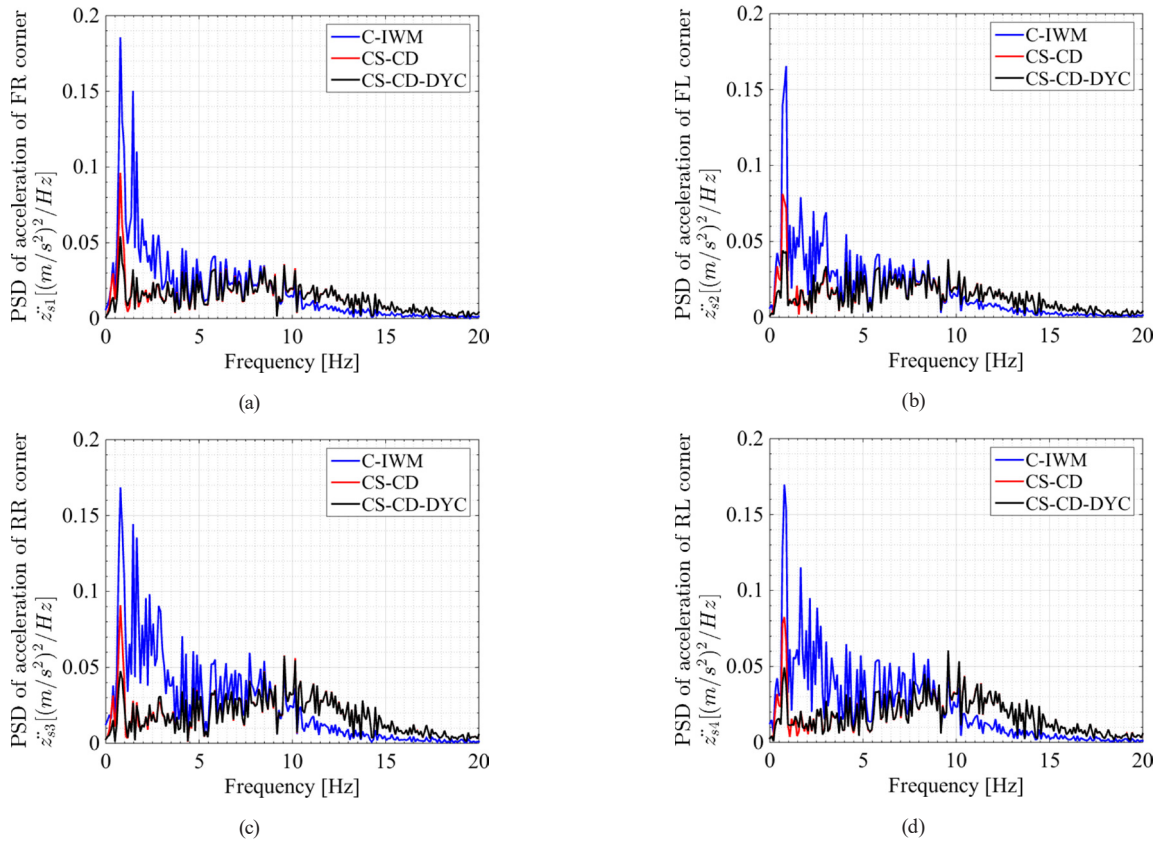


Fig. 11 Acceleration of each corner: (a) front right; (b) front left; (c) rear right; (d) rear left

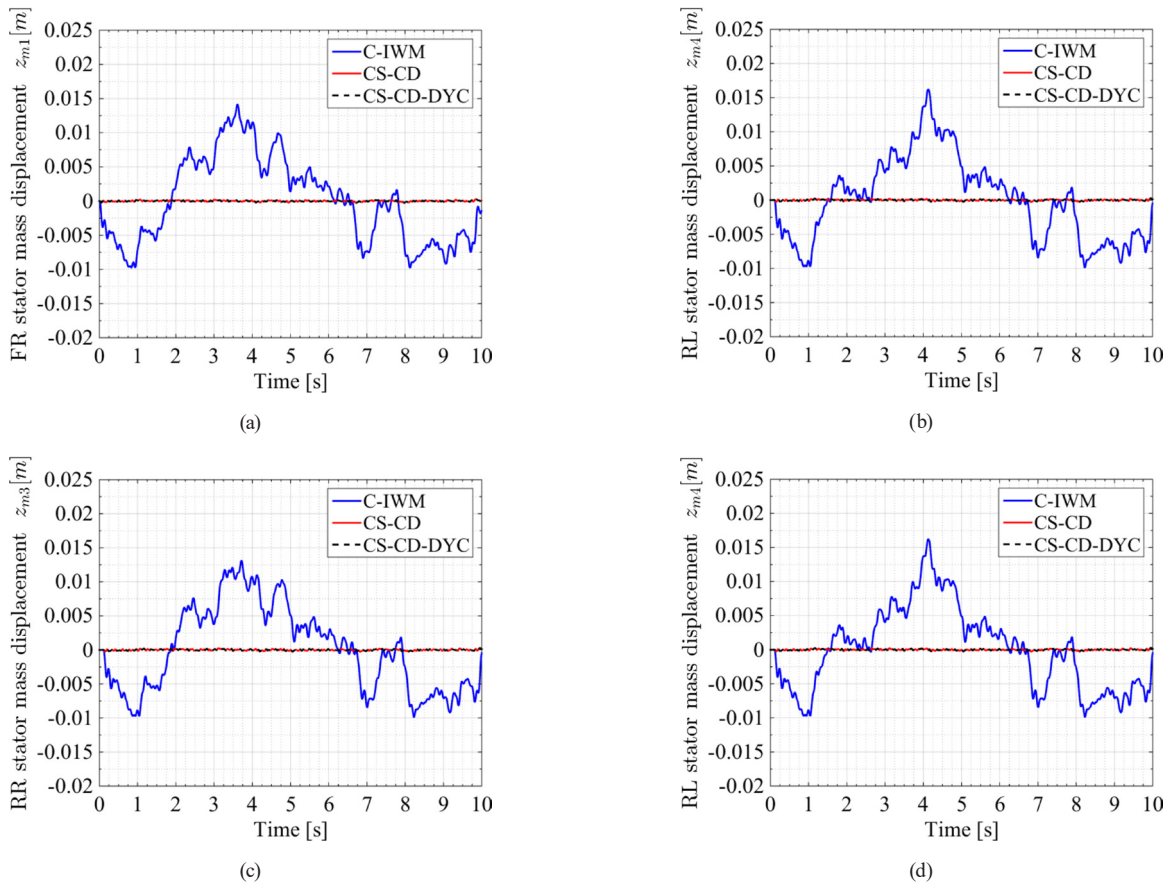


Fig. 12 Stator mass displacement: (a) front right; (b) front left; (c) rear right; (d) rear left

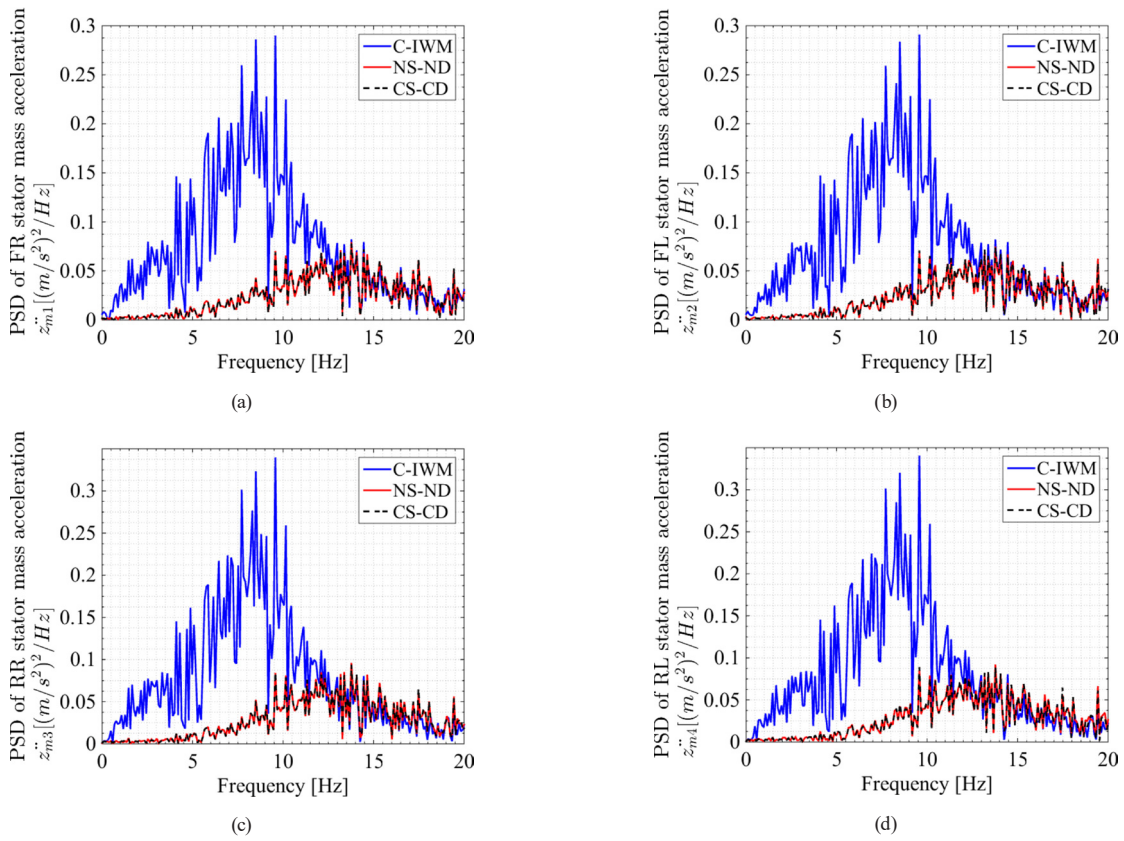


Fig. 13 Stator mass acceleration: (a) front right; (b) front left; (c) rear right; (d) rear left

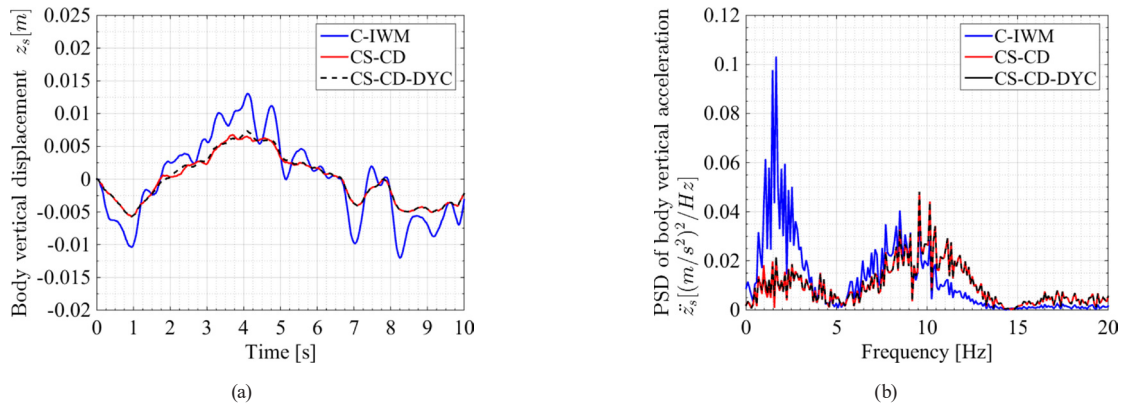


Fig. 14 (a) Body vertical displacement; (b) PSD of body vertical acceleration

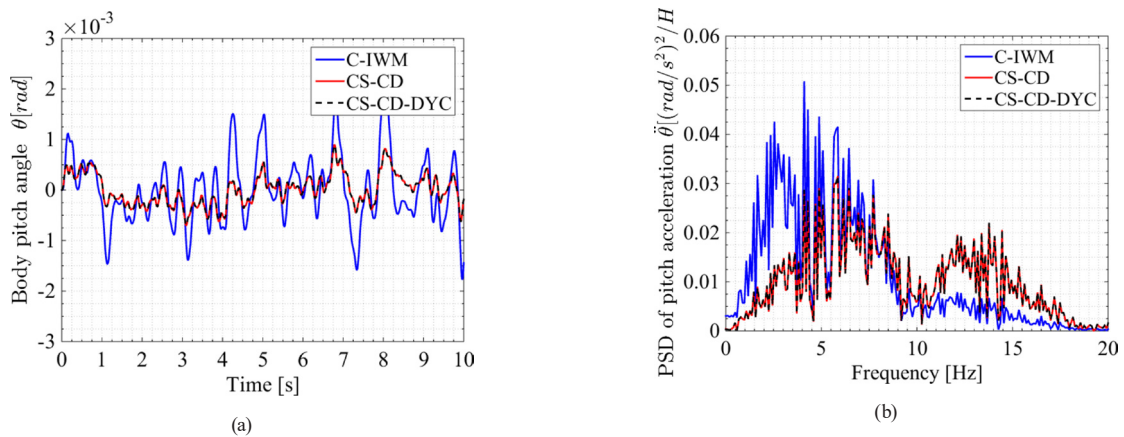


Fig. 15 (a) Body pitch angle; (b) PSD of body pitch acceleration

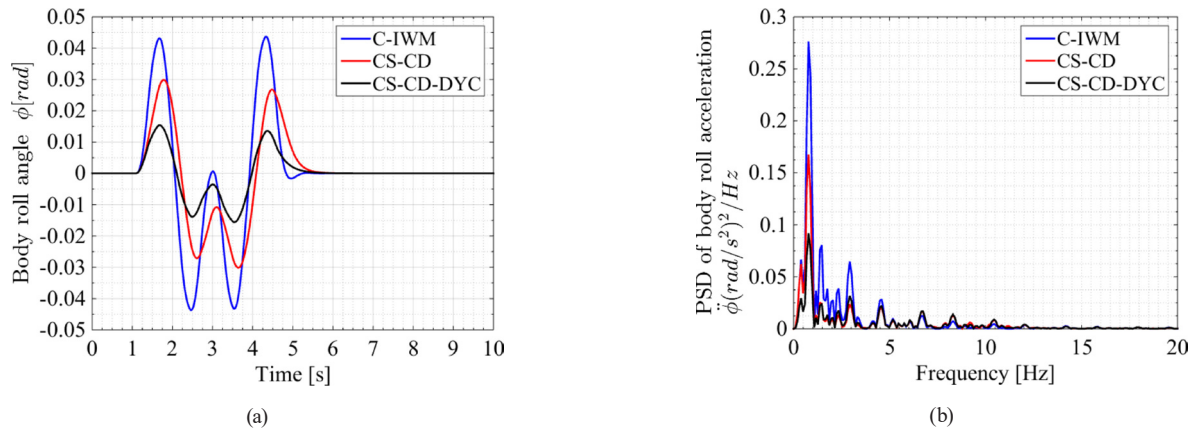


Fig. 16 (a) Body roll angle; (b) PSD of body roll acceleration

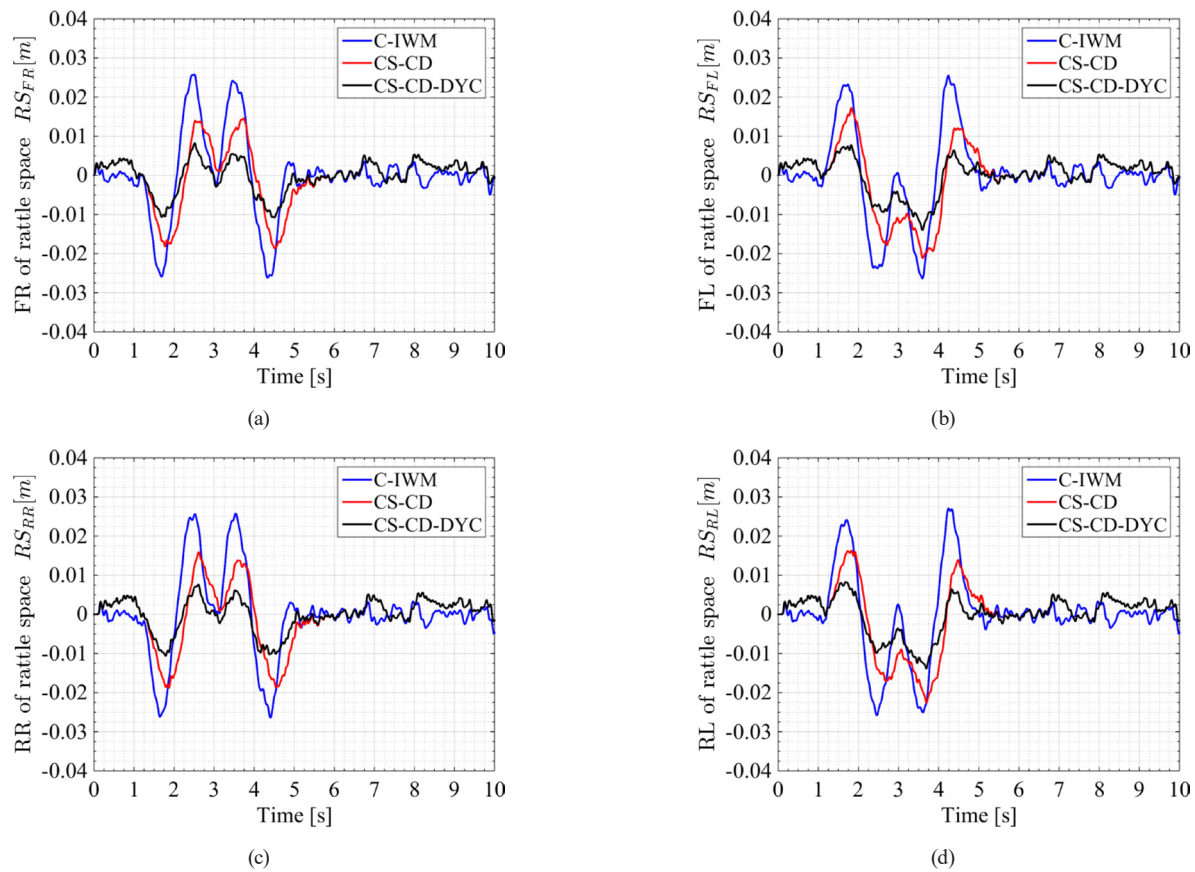


Fig. 17 Rattle space: (a) front right; (b) front left; (c) rear right; (d) rear left

compared to the C-IWM case. This indicates that the sliding mode control designed can significantly reduce the vibrations of all motors. We notice similar responses for the two cases CS-CD and CS-CD-DYC throughout the duration of the simulation. This indicates that the differential braking applied to the motors by the DYC does not conflict with the vibration absorption system control of the DVA motors. We also notice that CS-CD and CS-CD-DYC has slightly better performance compared to C-IWM, especially in the natural frequency of the electric wheel (in range of [8–11] Hz).

According to Fig. 14 and Table 6, we notice that the improvement of the vertical dynamics of each corner of the frame presented previously in Figs. 12 and 13, directly influences the improvement of the acceleration and vertical displacement of the gravity center of the vehicle body in the case of CS-CD versus C-IWM. In contrast, the CS-CD-DYC case has an almost similar response to the CS-CD case throughout the driving period. Fig. 14(b) shows the PSD of the GC vehicle body acceleration with a natural frequency of the vehicle body (in range of [1–2.5] Hz). Note

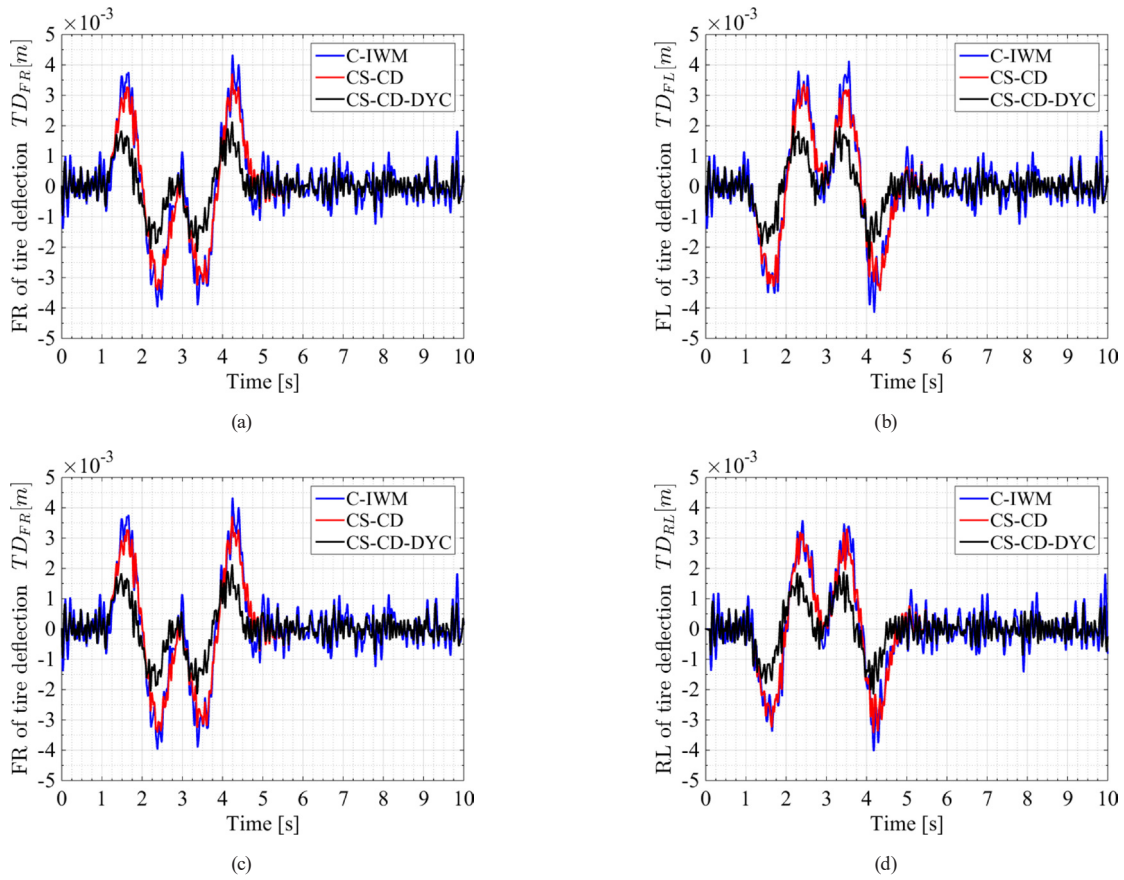


Fig. 18 Tire deflection: (a) front right; (b) front left; (c) rear right; (d) rear left

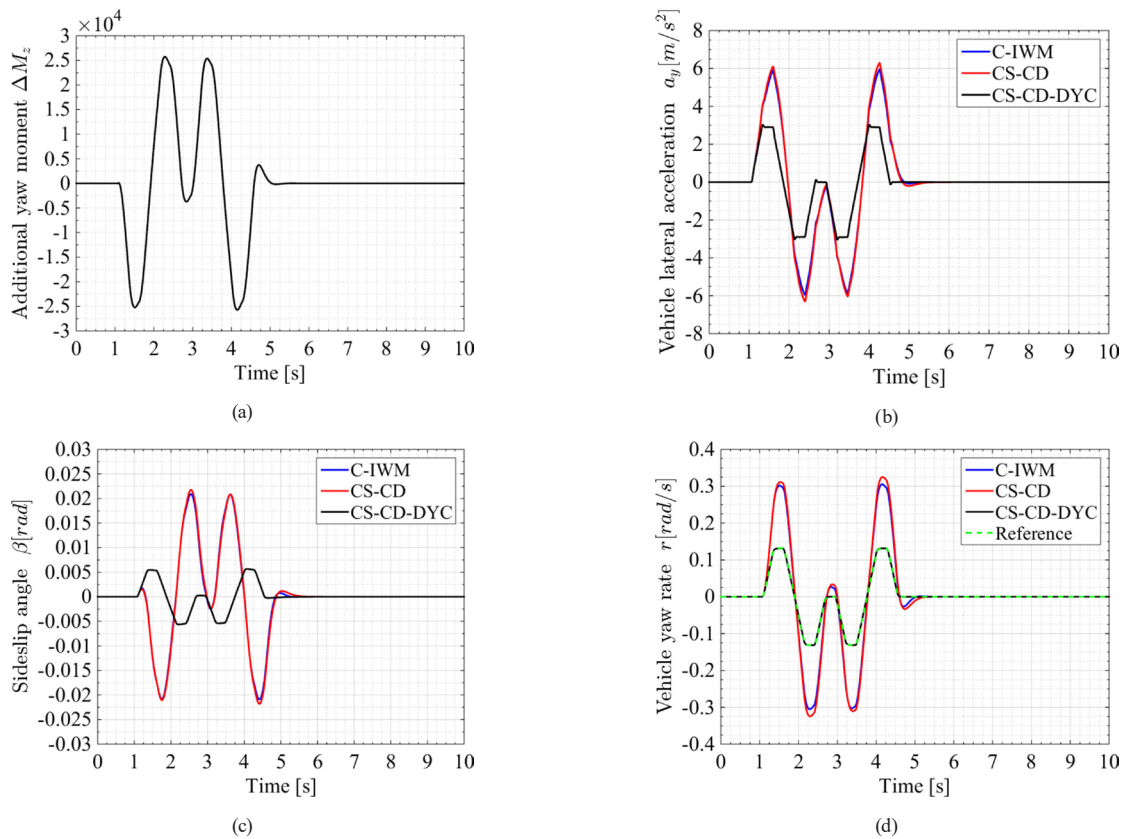


Fig. 19 (a) Additional yaw moment; (b) vehicle lateral acceleration; (c) sideslip angle; (d) vehicle yaw rate

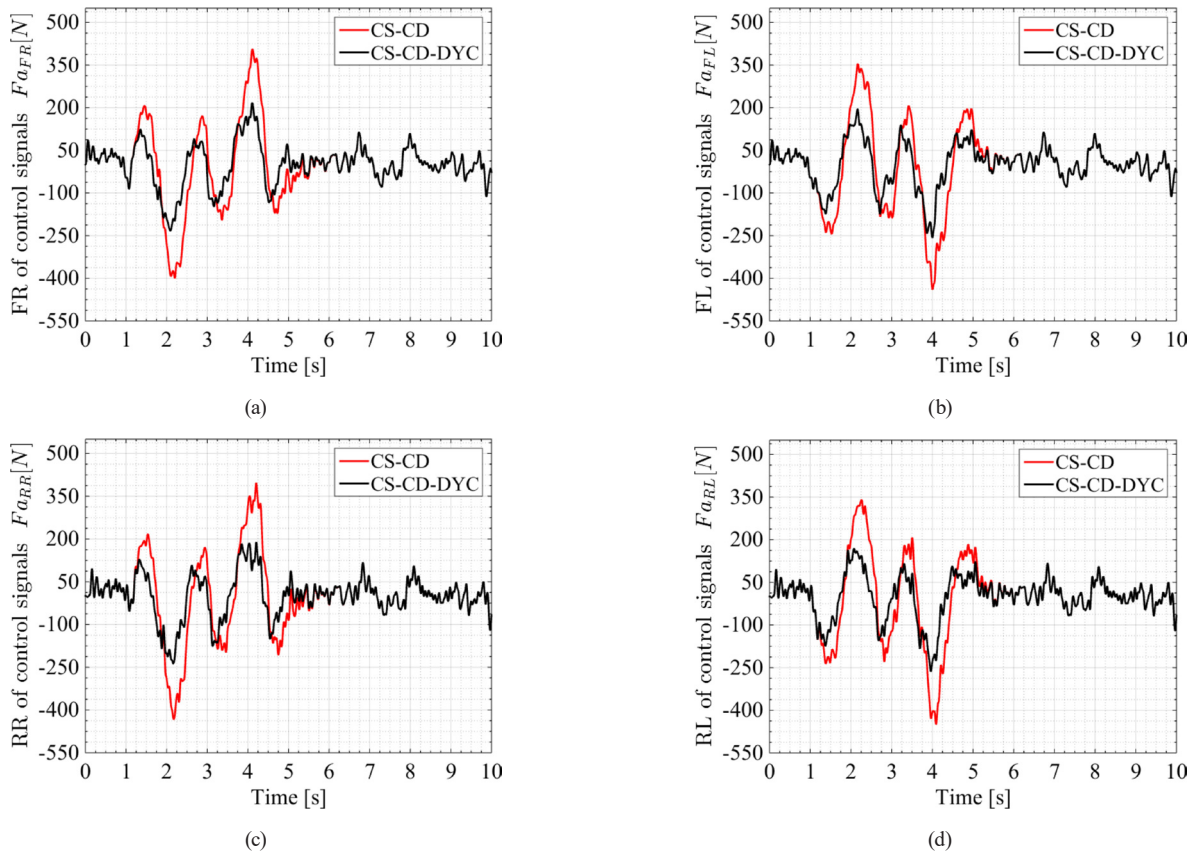


Fig. 20 Control signals for active suspension system: (a) front right; (b) front left; (c) rear right; (d) rear left

Table 4 The various situations that arise while driving

Period	Speed	Road profile	Steering angle
$t \in [0 \text{ } 4.5 \text{ sec}]$	80 km/h	Random road	A succession of turns
$t \in [4.5 \text{ } 10 \text{ sec}]$		excitation	Zero

Table 5 Natural frequencies of the suspension elements within the frequency range 1–11 Hz

Variables	Natural frequencies (Hz)	
	Calculated value	Estimated value through simulation
Body vertical acceleration	1.4335	[1–2.5]
Stator mass acceleration	8.8574	[8–11]
Pitch acceleration	3.6975	[3.5–5.5]
Roll acceleration	1.707	[0.5–2]

that CS-CD has a slightly better performance compared to C-IWM, especially in the natural frequency band.

Fig. 15 show the angle response in the time domain and the PSD of pitch acceleration with a natural frequency (in range of [3.5–5] Hz). Note that the improvement of the vertical dynamics of each body corner and the suppression of motor vibrations in the CS-CD case presented previously results in the improvement of the angle responses and the

pitch acceleration ( $\uparrow 22.709\%$ ) in the case CS-CD versus C-IWM. We also notice that the CS-CD-DYC case has an almost similar response to the CS-CD case with about ( $\uparrow 22.713\%$ ) improvement while the vehicle is moving, i.e. during the entire driving period. This is explained by the good distribution of forces by the DYC on the four motors, which prevents the increase in pitch angle and acceleration when applying differential braking to the motors. According to Fig. 15(b) the PSD of body pitch acceleration in the case CS-CD and CS-CD-DYC have slightly better performances compared to C-IWM, especially in the natural frequency band (in range of [3.5–5] Hz).

Fig. 16 show the time domain of roll angle and the PSD of roll acceleration. It is noticed that the improvement of the vertical dynamics of each body corner and the suppression of the vibrations of the motors in the CS-CD case by using the combined control between the Skyhook and the CSTA positively influence the angle responses and the roll acceleration in the CS-CD case with ( $\uparrow 40.92\%$ ) improvement compared to C-IWM. We also notice a significant improvement during the application of maneuvers in the case of CS-CD-DYC ( $\uparrow 63.711\%$ ), which explains why DYC plays its role well in reinforcing the lateral stability of the

**Table 6** RMS comparison of vehicle suspension under random road excitation

Vehicle performance (RMS)		Test		
		C-IWM	CS-CD	CS-CD-DYC
Criterion 1: Ride comfort	$SMA = \ddot{z}_s$	0.19995	0.12988 (↑35.043%)	0.12983 (↑35.066%)
	$RS_{FR} = z_{s1} - z_{w1}$	0.0099883	0.0070575 (↑29.343%)	0.0039594 (↑60.36%)
Criterion 2: Rattle space	$RS_{FL} = z_{s2} - z_{w2}$	0.009944	0.0077842 (↑21.719%)	0.0044822 (↑54.926%)
	$RS_{RR} = z_{s3} - z_{w3}$	0.0101	0.0072407 (↑28.31%)	0.0041282 (↑59.126%)
	$RS_{RL} = z_{s4} - z_{w4}$	0.010071	0.007981 (↑20.753%)	0.0046823 (↑53.507%)
	$TD_{FR} = z_{w1} - z_{r1}$	0.0014235	0.0012686 (↑10.876%)	0.0006952 (↑51.161%)
Criterion 3: Road holding	$TD_{FL} = z_{w2} - z_{r2}$	0.0014135	0.0012674 (↑10.333%)	0.0006927 (↑50.993%)
	$TD_{RR} = z_{w3} - z_{r3}$	0.0012825	0.0011872 (↑7.4303%)	0.00066222 (↑48.365%)
	$TD_{RL} = z_{w4} - z_{r4}$	0.0012742	0.0011842 (↑7.0625%)	0.00065768 (↑48.387%)
	$SA_{FR} = \ddot{z}_{m1}$	0.95888	0.3253 (↑66.075%)	0.32734 (↑65.863%)
Criterion 4: Stator acceleration	$SA_{FL} = \ddot{z}_{m2}$	0.96088	0.32369 (↑66.314%)	0.32645 (↑66.026%)
	$SA_{RR} = \ddot{z}_{m3}$	1.0481	0.37602 (↑63.927%)	0.37781 (↑63.953%)
	$SA_{RL} = \ddot{z}_{m4}$	1.046	0.37580 (↑64.0727%)	0.37754 (↑63.906%)
	$\ddot{z}_{s1}$	0.31747	0.18407 (↑42.02%)	0.16534 (↑47.918%)
Acceleration of each corner	$\ddot{z}_{s2}$	0.29662	0.18613 (↑37.249%)	0.16752 (↑43.524%)
	$\ddot{z}_{s3}$	0.3876	0.22883 (↑40.963%)	0.21396 (↑44.799%)
	$\ddot{z}_{s4}$	0.35209	0.22384 (↑36.426%)	0.20891 (↑40.666%)
	Body roll acceleration	$\ddot{\theta}$	0.16037	0.12395 (↑22.709%)
Body pitch acceleration	$\ddot{\phi}$	0.33771	0.19952 (↑40.92%)	0.12255 (↑63.711%)

vehicle. Note that CS-CD-DYC has slightly better performance compared to C-IWM and CS-CD, especially in the natural frequency band (in range of [0.5–2] Hz).

According to Figs. 17 and 18 and Table 6, the suspension deflection (RS) and the tire deflection (TD) (front left/right and rear left/right) are considerably reduced in the case of CS-CD compared to C-IWM. This indicates that the combined control for the vehicle's suspension system helps to ensure good handling. Therefore, tire and suspension deflection dynamics are improved with the addition of DYC. This indicates that the vehicle yaw moment control enhances lateral stability and increases suspension system performance, simultaneously.

We notice in Fig. 19 that throughout the maneuvers, the SMC-DYC controller provides an additional yaw moment (Fig. 19(a)), which decreases the lateral acceleration and the sideslip angle of the vehicle to ensure passenger comfort, as shown in the Fig. 19(b) and (c), respectively. Fig. 19(d) shows that the vehicle yaw rate follows its desired path despite vibrations resulting from road irregularities. This shows that the proposed SMC-DYC is working correctly.

The control signals in the CS-CD and CS-CD-DYC cases are shown in Fig. 20. The control force requirements for driving comfort and handling can be seen in Fig. 20. The suspension control signal in the CS-CD-DYC case, exhibits a relatively small change in frequency and amplitude compared

to the CS-CD case when the steering wheel maneuvers are applied during the period 1–4.5 sec. This indicates that there is good coordination between the three proposed controllers.

The simulation results show that several turns' maneuvers test under random road excitation have a significant impact on the vehicle's handling stability. Under these conditions, the suggested DYC system can keep the vehicle stable and enhance path tracking ability.

### 5 Conclusion

This paper focuses on the vertical and lateral coupling dynamics control for a four in-wheel motor drive electric vehicle, aiming at enhancing lateral stability, the rollover resistance performance, ride comfort and the road holding under critical driving conditions. To investigate the impact of these conditions (excitation sources) on vehicle vertical and lateral coupling dynamics, a 16-degree-of-freedom dynamics model was developed and verified. Furthermore, to improve the vehicle coupling dynamics, a proposed controller is designed based on the dynamic vibration absorber, active suspension, and direct yaw stability control. Two input conditions, namely the random road excitation input and the steering angle input are applied to evaluate the lateral stability of the vehicle suspension performance and improve the rollover resistance performance. Simulations under these driving conditions

are carried out to verify the proposed control. The simulation results show that the proposed advanced vertical and lateral coupling dynamics control may increase the ride comfort, road holding, and lateral stability of the vehicle suspension system simultaneously without having a

contradicting effect between the vertical and lateral controllers. This research can give a theoretical basis for the design of the four in-wheel motor drive electric vehicles with combined lateral and vertical control.

## References

- [1] Sekour, M., Hartani, K., Merah, A. "Electric Vehicle Longitudinal Stability Control Based on a New Multimachine Nonlinear Model Predictive Direct Torque Control", *Journal of Advanced Transportation*, 2017, 4125384, 2017.  
<https://doi.org/10.1155/2017/4125384>
- [2] Hori, Y. "Future vehicle driven by electricity and control-research on four-wheel-motored "UOT Electric March II", *IEEE Transactions on Industrial Electronics*, 51(5), pp. 954–962, 2004.  
<https://doi.org/10.1109/TIE.2004.834944>
- [3] Doumiati, M., Sename, O., Dugard, L., Martinez-Molina, J.-J., Gaspar, P., Szabo, Z. "Integrated vehicle dynamics control via coordination of active front steering and rear braking", *European Journal of Control*, 19(2), pp. 121–143, 2013.  
<https://doi.org/10.1016/j.ejcon.2013.03.004>
- [4] Aouadj, N., Hartani, K., Fatiha, M. "New Integrated Vehicle Dynamics Control System Based on the Coordination of Active Front Steering, Direct Yaw Control, and Electric Differential for Improvements in Vehicle Handling and Stability", *SAE International Journal of Vehicle Dynamics, Stability, and NVH*, 4(2), pp. 119–133, 2020.  
<https://doi.org/10.4271/10-04-02-0009>
- [5] Direm, C., Hartani, K., Aouadj, N. "New Combined Maximum Torque per Ampere-Flux Weakening Control Strategy for Vehicle Propulsion System", *SAE International Journal of Vehicle Dynamics, Stability, and NVH*, 5(2), pp. 131–145, 2021.  
<https://doi.org/10.4271/10-05-02-0009>
- [6] El djallil Rabhi, A., Hartani, K., Guettaf, Y., Norediene, A. "Robust Multimachine Control for Bisynchronous Propulsion Traction Chain of an Electric Vehicle", *SAE International Journal of Vehicle Dynamics, Stability, and NVH*, 5(2), pp. 173–189, 2021.  
<https://doi.org/10.4271/10-05-02-0012>
- [7] Qin, Y., He, C., Ding, P., Dong, M., Huang, Y. "Suspension hybrid control for in-wheel motor driven electric vehicle with dynamic vibration absorbing structures", *IFAC-PapersOnLine*, 51(31), pp. 973–978, 2018.  
<https://doi.org/10.1016/j.ifacol.2018.10.054>
- [8] Tan, D., Lu, C. "The influence of the magnetic force generated by the in-wheel motor on the vertical and lateral coupling dynamics of electric vehicles", *IEEE Transactions on Vehicular Technology*, 65(6), pp. 4655–4668, 2016.  
<https://doi.org/10.1109/TVT.2015.2461635>
- [9] Liu, M., Gu, F., Zhang, Y. "Ride comfort optimization of in-wheel-motor electric vehicles with in-wheel vibration absorbers", *Energies*, 10(10), 1647, 2017.  
<https://doi.org/10.3390/en10101647>
- [10] Nie, S., Zhuang, Y., Chen, F., Wang, Y., Liu, S. "A method to eliminate unsprung adverse effect of in-wheel motor-driven vehicles", *Journal of Low Frequency Noise, Vibration and Active Control*, 37(4), pp. 955–976, 2018.  
<https://doi.org/10.1177/1461348418767096>
- [11] Qin, Y., He, C., Shao, X., Du, H., Xiang, C., Dong, M. "Vibration mitigation for in-wheel switched reluctance motor driven electric vehicle with dynamic vibration absorbing structures", *Journal of Sound and Vibration*, 419, pp. 249–267, 2018.  
<https://doi.org/10.1016/j.jsv.2018.01.010>
- [12] Sun, W., Li, Y., Huang, J., Zhang, N. "Vibration effect and control of in-wheel switched reluctance motor for electric vehicle", *Journal of Sound and Vibration*, 338, pp. 105–120, 2015.  
<https://doi.org/10.1016/j.jsv.2014.10.036>
- [13] Omar, A. A. A., Özkan, B. "Evaluation of effect of in-wheel electric motors mass on the active suspension system performance using linear quadratic regulator control method", *International Journal of Innovative Research in Science, Engineering and Technology*, 4(1), pp. 18655–18663, 2015.  
<https://doi.org/10.15680/IJRSET.2015.0401043>
- [14] van der Westhuizen, S. F., Els, P. S. "Slow active suspension control for rollover prevention", *Journal of Terramechanics*, 50(1), pp. 29–36, 2013.  
<https://doi.org/10.1016/j.jterra.2012.10.001>
- [15] Rajeswari, K., Lakshmi, P. "PSO optimized fuzzy logic controller for active suspension system", In: *2010 International Conference on Advances in Recent Technologies in Communication and Computing*, Kottayam, India, 2010, pp. 278–283. ISBN 978-1-4244-8093-7  
<https://doi.org/10.1109/ARTCom.2010.22>
- [16] Qazi, A. J., de Silva, C. W., Khan, A., Khan, M. T. "Performance analysis of a semiactive suspension system with particle swarm optimization and fuzzy logic control", *The Scientific World Journal*, 2014, 174102, 2014.  
<https://doi.org/10.1155/2014/174102>
- [17] Qamar, S., Khan, T., Khan, L. "Adaptive neuro-fuzzy sliding mode control based strategy for active suspension control", In: *2012 10th International Conference on Frontiers of Information Technology*, Islamabad, Pakistan, 2012, pp. 107–115. ISBN 978-1-4673-4946-8  
<https://doi.org/10.1109/FIT.2012.28>
- [18] Deshpande, V. S., Bhaskara, M., Phadke, S. B. "Sliding mode control of active suspension systems using a disturbance observer", In: *2012 12th International Workshop on Variable Structure Systems*, Mumbai, India, 2012, pp. 70–75. ISBN 978-1-4577-2066-6  
<https://doi.org/10.1109/VSS.2012.6163480>
- [19] Basturk, H. I. "A backstepping approach for an active suspension system", In: *2016 American Control Conference (ACC)*, Boston, MA, USA, 2016, pp. 7579–7584. ISBN 978-1-4673-8683-8  
<https://doi.org/10.1109/ACC.2016.7526870>
- [20] Deshpande, V. S., Shendge, P. D., Phadke, S. B. "Nonlinear control for dual objective active suspension systems", *IEEE Transactions on Intelligent Transportation Systems*, 18(3), pp. 656–665, 2017.  
<https://doi.org/10.1109/TITS.2016.2585343>

- [21] Pan, Y., Du, P., Xue, H., Lam, H.-K. "Singularity-free fixed-time fuzzy control for robotic systems with user-defined performance", *IEEE Transactions on Fuzzy Systems*, 29(8), pp. 2388–2398, 2021. <https://doi.org/10.1109/TFUZZ.2020.2999746>
- [22] Liang, H., Liu, G., Huang, T., Lam, H.-K., Wang, B. "Cooperative fault-tolerant control for networks of stochastic nonlinear systems with nondifferential saturation nonlinearity", *IEEE Transactions on Systems, Man, and Cybernetics: Systems*, 52(3), pp. 1362–1372, 2022. <https://doi.org/10.1109/TSMC.2020.3020188>
- [23] Shtessel, Y., Edwards, C., Fridman, L., Levant, A. "Conventional sliding mode observers", In: *Sliding Mode Control and Observation*, Birkhäuser, 2014, pp. 105–141. ISBN 978-0-8176-4892-3 [https://doi.org/10.1007/978-0-8176-4893-0\\_3](https://doi.org/10.1007/978-0-8176-4893-0_3)
- [24] Utkin, V. I. "Sliding Modes in Control and Optimization", Springer, 1992. ISBN 978-3-642-84381-5 <https://doi.org/10.1007/978-3-642-84379-2>
- [25] Ahmed, H., Ríos, H. "Experimental study of robust output-based continuous sliding-modes controllers for Van der Pol oscillator", *IET Control Theory & Applications*, 12(15), pp. 2088–2097, 2018. <https://doi.org/10.1049/iet-cta.2017.1142>
- [26] Moreno, J. A. "Discontinuous integral control for systems with relative degree two", In: Clempner, J. B., Yu, W. (eds.) *New Perspectives and Applications of Modern Control Theory: In Honor of Alexander S. Poznyak*, Springer, 2018, pp. 187–218. ISBN 978-3-319-62463-1 <https://doi.org/10.1007/978-3-319-62464-88>
- [27] Zhu, Y., Bian, X., Chen, D., Su, L., Li, F., Shi, Y., Jin, T. "Vertical and Longitudinal Coupling Control Approach for Semi-active Suspension System Using Mechanical Hardware-in-the-Loop Simulation", *SAE International Journal of Vehicle Dynamics, Stability, and NVH*, 5(2), pp. 147–158, 2021. <https://doi.org/10.4271/10-05-02-0010>
- [28] Zhu, Y., Bian, X., Su, L., Gu, C., Wang, Z., Shi, C. "Ride Comfort Improvement with Preview Control Semi-active Suspension System Based on Supervised Deep Learning", *SAE International Journal of Vehicle Dynamics, Stability, and NVH*, 5(1), pp. 31–44, 2021. <https://doi.org/10.4271/10-05-01-0003>
- [29] Shao, X., Naghdy, F., Du, H. "Reliable fuzzy  $H_\infty$  control for active suspension of in-wheel motor driven electric vehicles with dynamic damping", *Mechanical Systems and Signal Processing*, 87, pp. 365–383, 2017. <https://doi.org/10.1016/j.ymssp.2016.10.032>
- [30] Chen, X., Yin, J., Wang, W., Wu, L., and Tang, F. "Approaches to diminish large unsprung mass negative effects of wheel side drive electric vehicles", *Journal of Advanced Mechanical Design, Systems, and Manufacturing*, 10(4), JAMDSM0064, 2016. <https://doi.org/10.1299/jamdsm.2016jamdsm0064>
- [31] Liu, M., Gu, F., Huang, J., Wang, C., Cao, M. "Integration design and optimization control of a dynamic vibration absorber for electric wheels with in-wheel motor", *Energies*, 10(12), 2069, 2017. <https://doi.org/10.3390/en10122069>
- [32] Li, W., Xie, Z., Wong, P. K., Cao, Y., Hua, X., Zhao, J. "Robust nonfragile  $H_\infty$  optimum control for active suspension systems with time-varying actuator delay", *Journal of Vibration and Control*, 25(18), pp. 2435–2452, 2019. <https://doi.org/10.1177/1077546319857338>
- [33] Yatak, M. Ö., Şahin, F. "Ride Comfort-Road Holding Trade-off Improvement of Full Vehicle Active Suspension System by Interval Type-2 Fuzzy Control", *Engineering Science and Technology, an International Journal*, 24(1), pp. 259–270, 2021. <https://doi.org/10.1016/j.jestch.2020.10.006>
- [34] Rajamani, R. "Vehicle Dynamics and Control", Springer, 2012. ISBN 978-1-4614-1432-2 <https://doi.org/10.1007/978-1-4614-1433-9>
- [35] Wang, R., Jing, H., Yan, F., Karimi, H. R., Chen, N. "Optimization and finite-frequency  $H_\infty$  control of active suspensions in in-wheel motor driven electric ground vehicles", *Journal of the Franklin Institute*, 352(2), pp. 468–484, 2015. <https://doi.org/10.1016/j.franklin.2014.05.005>
- [36] Fridman, L., Moreno, J. A., Bandyopadhyay, B., Kamal, S., Chalanga, A. "Continuous nested algorithms: The fifth generation of sliding mode controllers", In: Yu, X., Önder Efe, M. (eds.) *Recent Advances in Sliding Modes: From Control to Intelligent Mechatronics*, Springer, 2015, pp. 5–35. ISBN 978-3-319-18289-6 [https://doi.org/10.1007/978-3-319-18290-2\\_2](https://doi.org/10.1007/978-3-319-18290-2_2)
- [37] Ovalle, L., Ríos, H., Ahmed, H. "Robust Control for an Active Suspension System via Continuous Sliding-Mode Controllers", *Engineering Science and Technology, an International Journal*, 28, 101026, 2022. <https://doi.org/10.1016/j.jestch.2021.06.006>
- [38] Pérez-Ventura, U., Fridman, L. "When is it reasonable to implement the discontinuous sliding-mode controllers instead of the continuous ones? Frequency domain criteria", *International Journal of Robust and Nonlinear Control*, 29(3), pp. 810–828, 2019. <https://doi.org/10.1002/rnc.4347>
- [39] Payghan, V. S., Shendge, P. D., Yerge, R. M., Phadke, S. B. "Skyhook control for active suspension system with a novel variable damper", In: *2017 2nd IEEE International Conference on Recent Trends in Electronics, Information & Communication Technology (RTEICT)*, Bangalore, India, 2017, pp. 725–729. ISBN 978-1-5090-3705-6 <https://doi.org/10.1109/RTEICT.2017.8256692>
- [40] Nguyen, N. T. "Lyapunov Stability Theory", In: *Model-Reference Adaptive Control*, Springer, 2018, pp. 47–81. ISBN 978-3-319-56392-3 [https://doi.org/10.1007/978-3-319-56393-0\\_4](https://doi.org/10.1007/978-3-319-56393-0_4)
- [41] Shen, Y., Chen, L., Liu, Y., Zhang, X., Yang, X. "Improvement of the lateral stability of vehicle suspension incorporating inerter", *Science China Technological Sciences*, 61(8), pp. 1244–1252, 2018. <https://doi.org/10.1007/s11431-017-9228-0>
- [42] Cao, D., Song, X., Ahmadian, M. "Editors' perspectives: road vehicle suspension design, dynamics, and control", *Vehicle System Dynamics*, 49(1–2), pp. 3–28, 2011. <https://doi.org/10.1080/00423114.2010.532223>
- [43] Qin, Y., Wang, H., Huang, Y., Tang, X. "Real-Time Road Profile Identification and Monitoring: Theory and Application", Springer Nature, 2019. ISBN 978-3-031-00004-1 <https://doi.org/10.1007/978-3-031-01499-4>
- [44] International Organization for Standardization "ISO 8601 Date and time format", International Organization for Standardization, Geneva, Switzerland, 2016.

- [45] International Organization for Standardization "ISO 8608:2016 Mechanical vibration — Road surface profiles — Reporting of measured data", International Organization for Standardization, Geneva, Switzerland, 2016.
- [46] Zhang, B., Zhang, J., Yi, J., Zhang, N., Jin, Q. "Modal and dynamic analysis of a vehicle with kinetic dynamic suspension system", Shock and Vibration, 2016, 5239837, 2016.  
<https://doi.org/10.1155/2016/5239837>